

Kaon Condensation in Neutron Stars with Skyrme-Hartree-Fock Models

Yeunhwan Lim,^{1,2,*} Kyujin Kwak,^{3,†} Chang Ho Hyun,^{1,‡} and Chang-Hwan Lee^{4,5,§}

¹*Department of Physics Education, Daegu University,
Gyeongsan 712-714, Republic of Korea*

²*Rare Isotope Science Project, Institute for Basic Science,
Daejeon 305-811, Republic of Korea*

³*School of Natural Science, Ulsan National Institute of Science
and Technology (UNIST), Ulsan 689-798, Republic of Korea*

⁴*Department of Physics, Pusan National University, Busan 609-735, Republic of Korea*

⁵*Department of Physics and Astronomy,
State University of New York at Stony Brook, Stony Brook, NY 11794, USA*

(Dated: May 13, 2014)

Abstract

We investigate nuclear matter equations of state in neutron star with kaon condensation. It is generally known that the existence of kaons in neutron star makes the equation of state soft so that the maximum mass of neutron star is not likely to be greater than $2.0 M_{\odot}$, the maximum mass constrained by current observations. With existing Skyrme force model parameters, we calculate nuclear equations of state and check the possibility of kaon condensation in the core of neutron stars. The results show that even with the kaon condensation, the nuclear equation of state satisfies both the maximum mass and the allowed ranges of mass and radius.

PACS numbers: 97.60.Jd, 21.30.-x, 13.75.Jz

*Electronic address: ylim9057@ibs.re.kr

†Electronic address: kkwak@unist.ac.kr

‡Electronic address: hch@daegu.ac.kr

§Electronic address: clee@pusan.ac.kr

I. INTRODUCTION

Theory of nuclear matter has been tested using the properties of the observed nuclei whose number amounts to approximately 3,000 to date. The Skyrme-Hartree-Fock (SHF) models have been widely used to describe the general properties of nuclear medium and heavy nuclei in the non-relativistic limit. However, depending on the selection of the data and the methods to fit the model parameters, there are now more than 100 SHF models, and new models are still in birth due to the continuous update of the data. Although most of the SHF models even with different model parameters can explain the properties of numerous known nuclei consistently, predictions on the properties of the infinite nuclear matter strongly depend on the models, especially at high densities far above the nuclear saturation density ρ_0 ($\sim 0.16 \text{ fm}^{-3}$) [1]. As a result, the maximum mass of stable neutron stars calculated with known SHF models ranges from $1.4M_\odot$ to $2.5M_\odot$ where M_\odot is the solar mass [2].

At the core of neutron stars, there can be significant contributions from the exotic states, such as strangeness condensates, meson condensates, strange quark matter, etc., which are quite uncertain. The effect of strange particles, such as hyperons, on the nuclear matter equation of state (EoS) has been studied within the SHF models [3, 4]. In these works the existence of hyperons softens the nuclear matter EoS substantially and as a consequence the maximum mass of the neutron star decreases. Similar conclusion for the effect of hyperons has been drawn from the calculations done with the relativistic mean field models (for example, see [5]).

Recently $2M_\odot$ neutron stars in neutron star-white dwarf binaries were observed in pulsars PSR J1614–2230 [6] and PSR J0348+0432 [7]. This implies that any realistic EoS for the stable neutron star should be able to explain masses equal to or more than these values. With this criterion, SHF models predicting maximum masses to be less than $2M_\odot$ can be excluded from the candidates for the realistic models of high-density nuclear matter.

In this work, we revisit the kaon condensation and investigate its effect on the EoS of neutron star matter. In general, the EoS is very sensitive to the interactions of kaons in nuclear medium [8]. Since general SHF models do not include inherent kaon interactions in them, we need to import kaon interactions from other theories or models. In this work, we consider the SU(3) non-linear chiral effective model with kaons. We investigate how the

parameters in SHF and kaon interaction model affect the mass and radius of neutron stars, and constrain the parameter space by comparing our results with observed neutron star masses, $(1.97 \pm 0.04)M_\odot$ of PSR J1614–2230 and $(2.01 \pm 0.04)M_\odot$ of PSR J0348+0432.

This paper is organized as follows. In Sect. II, we describe the SHF models that we choose and the SU(3) non-linear chiral model for the interactions of kaons. In the same section, we derive basic equations from which the EoS within neutron stars is calculated. In Sect. III, we present our results on EoS, particle fractions, and mass-radius relations of neutron stars. Our conclusion and discussion are given in Sect. IV.

II. MODELS

A. SHF models

The general Skyrme force model is used to generate energy density functional (EDF), in which the effective two body force between nucleons is introduced. Because EDFs have been quite successful in explaining the properties of finite heavy nuclei, they have been also applied to the infinite dense system such as the interior of neutron stars. In the Skyrme type potential model, the effective interaction is given by

$$\begin{aligned}
v_{ij} = & t_0(1 + x_0 P_\sigma) \delta(\mathbf{r}_i - \mathbf{r}_j) + \frac{1}{2} t_1 (1 + x_1 P_\sigma) \frac{1}{\hbar^2} [\mathbf{p}_{ij}^2 \delta(\mathbf{r}_i - \mathbf{r}_j) + \delta(\mathbf{r}_i - \mathbf{r}_j) \mathbf{p}_{ij}^2] \\
& + t_2 (1 + x_2 P_\sigma) \frac{1}{\hbar^2} \mathbf{p}_{ij} \cdot \delta(\mathbf{r}_i - \mathbf{r}_j) \mathbf{p}_{ij} + \frac{1}{6} t_3 (1 + x_3 P_\sigma) \rho^\epsilon(\mathbf{r}) \delta(\mathbf{r}_i - \mathbf{r}_j) \\
& + \frac{i}{\hbar^2} W_0 \mathbf{p}_{ij} \cdot \delta(\mathbf{r}_i - \mathbf{r}_j) (\boldsymbol{\sigma}_i + \boldsymbol{\sigma}_j) \times \mathbf{p}_{ij},
\end{aligned} \tag{1}$$

where $\mathbf{r} = (\mathbf{r}_i + \mathbf{r}_j)/2$, $\mathbf{p}_{ij} = -i\hbar(\nabla_i - \nabla_j)/2$, P_σ is the spin-exchange operator, and $\rho(\mathbf{r}) = \rho_n(\mathbf{r}) + \rho_p(\mathbf{r})$. Using the Skyrme force model, the Hamiltonian density of nuclei can be written as [9]

$$\mathcal{H}_N = \mathcal{H}_B + \mathcal{H}_g + \mathcal{H}_C + \mathcal{H}_J. \tag{2}$$

The bulk Hamiltonian density is given by

$$\begin{aligned}
\mathcal{H}_B = & \frac{\hbar^2}{2M}\tau_n + \frac{\hbar^2}{2M}\tau_p + \rho(\tau_n + \tau_p) \left[\frac{t_1}{4} \left(1 + \frac{x_1}{2} \right) + \frac{t_2}{4} \left(1 + \frac{x_2}{2} \right) \right] \\
& + (\tau_n \rho_n + \tau_p \rho_p) \left[\frac{t_2}{4} \left(\frac{1}{2} + x_2 \right) - \frac{t_1}{4} \left(\frac{1}{2} + x_1 \right) \right] \\
& + \frac{t_0}{2} \left[\left(1 + \frac{x_0}{2} \right) \rho^2 - \left(\frac{1}{2} + x_0 \right) (\rho_n^2 + \rho_p^2) \right] \\
& + \frac{t_3}{12} \left[\left(1 + \frac{x_3}{2} \right) \rho^2 - \left(\frac{1}{2} + x_3 \right) (\rho_n^2 + \rho_p^2) \right] \rho^\epsilon.
\end{aligned} \tag{3}$$

The gradient Hamiltonian density takes the form of

$$\mathcal{H}_g = \frac{1}{2} Q_{nn} (\nabla \rho_n)^2 + Q_{np} \nabla \rho_n \cdot \nabla \rho_p + \frac{1}{2} Q_{pp} (\nabla \rho_p)^2, \tag{4}$$

with

$$\begin{aligned}
Q_{nn} = Q_{pp} &= \frac{3}{16} [t_1(1 - x_1) - t_2(1 + x_2)], \\
Q_{np} &= \frac{1}{8} \left[3t_1 \left(1 + \frac{x_1}{2} \right) - t_2 \left(1 + \frac{x_2}{2} \right) \right].
\end{aligned} \tag{5}$$

The Coulomb energy density is given by

$$\mathcal{H}_C = \frac{e^2}{2} \rho_n(\mathbf{r}) \int d^3r' \frac{\rho_p(\mathbf{r}')}{|\mathbf{r} - \mathbf{r}'|} - \frac{3e^2}{4} \left(\frac{3}{\pi} \right)^{1/3} \rho_p^{4/3}(\mathbf{r}), \tag{6}$$

and H_J comes from the spin-orbit interaction and is given by

$$\begin{aligned}
\mathcal{H}_J = & -\frac{W_0}{2} (\rho_n \nabla \cdot \mathbf{J}_n + \rho_p \nabla \cdot \mathbf{J}_p + \rho \nabla \cdot \mathbf{J}) \\
& + \frac{t_1}{16} (\mathbf{J}_n^2 + \mathbf{J}_p^2 - x_1 \mathbf{J}^2) - \frac{t_2}{16} (\mathbf{J}_n^2 + \mathbf{J}_p^2 + x_2 \mathbf{J}^2),
\end{aligned} \tag{7}$$

where $\mathbf{J}_{n(p)} = \sum_i \psi_{i,n(p)}^\dagger \boldsymbol{\sigma} \times \nabla \psi_{i,n}$ is the neutron (proton) spin-orbit density, and $\mathbf{J} = \mathbf{J}_n + \mathbf{J}_p$.

In general, ten independent parameters ($x_{i=0,1,2,3}$, $t_{i=0,1,2,3}$, ϵ , W_0) in Hamiltonian density are fixed by the properties of finite nuclei [10]. With the ten parameters fixed, we calculate the nuclear matter properties of the infinite nuclear matter (such as neutron stars) which determine the maximum mass of neutron stars. In this work, we employ four SHF models all of which predict the maximum mass of neutron stars larger than $2M_\odot$ while each model shows distinct characteristics for the symmetric nuclear matter properties and the stiffness of the EoS.

Table I summarizes nuclear matter properties and the maximum mass of neutron stars obtained from the four SHF models. For the four models that we select, the basic saturation

Model	ρ_0	B	S_v	L	K	m_N^*/m_N	M_{\max}/M_\odot
SLy4	0.160	16.0	32.0	45.9	230	0.694	2.07
SkI4	0.160	16.0	29.5	60.4	248	0.649	2.19
SGI	0.155	15.9	28.3	63.9	262	0.608	2.25
SV	0.155	16.1	32.8	96.1	306	0.383	2.44

TABLE I: Nuclear matter properties and the maximum mass of neutron star calculated from four SHF models that we select. ρ_0 : saturation density in unit of fm^{-3} , B : binding energy of the symmetric nuclear matter in unit of MeV, S_v : symmetry energy at the saturation density in unit of MeV, L : slope of symmetry energy at the saturation density in unit of MeV, K : compression modulus of the symmetric matter at the saturation density in unit of MeV, m_N^*/m_N : ratio of the effective mass of the nucleon at the saturation density (m_N^*) to the free mass of the nucleon (m_N), and M_{\max}/M_\odot : maximum mass of neutron star in unit of the solar mass (M_\odot).

properties ρ_0 and B are almost identical or similar to each other, but the values of S_v , L and K vary significantly from model to model even though they are in the range of general acceptance. Note that larger K causes stiffer EoS. The table confirms that the maximum mass of neutron star increases with K .

B. Kaon interactions

Several models describe the interaction of kaon in nuclear medium. As for two examples, kaonic optical potential treats kaon interaction phenomenologically and the meson-exchange model mediates the interaction of the kaon with the background nuclear matter [11]. In this work, we employ a SU(3) non-linear chiral model which was first proposed by Kaplan and Nelson [12]. The effective chiral Lagrangian density is given as

$$\begin{aligned}
\mathcal{L} = & \frac{f_\pi^2}{4} \text{Tr} \partial_\mu U \partial^\mu U^\dagger + c \text{Tr} [m_q (U + U^\dagger - 2)] + i \text{Tr} \bar{B} \gamma^\mu \partial_\mu B \\
& + i \text{Tr} B^\dagger [V_0, B] - D \text{Tr} B^\dagger \boldsymbol{\sigma} \cdot \{\mathbf{A}, B\} - F \text{Tr} B^\dagger \boldsymbol{\sigma} \cdot [\mathbf{A}, B] \\
& + a_1 \text{Tr} B^\dagger (\xi m_q \xi + \text{h.c.}) B + a_2 \text{Tr} B^\dagger B (\xi m_q \xi + \text{h.c.}) + a_3 \text{Tr} B^\dagger B \text{Tr} (m_q U + \text{h.c.}), \quad (8)
\end{aligned}$$

where f_π is the pion decay constant ($\simeq 93$ MeV). Chiral fields U and ξ are defined by

$$U = \xi^2 = \exp(\sqrt{2}iM/f_\pi), \quad (9)$$

and the mesonic vector and axial currents read

$$V_\mu = \frac{1}{2} (\xi^\dagger \partial_\mu \xi + \xi \partial_\mu \xi^\dagger), \quad A_\mu = \frac{i}{2} (\xi^\dagger \partial_\mu \xi - \xi \partial_\mu \xi^\dagger). \quad (10)$$

The meson and baryon octet fields M and B are defined as

$$M = \begin{pmatrix} \frac{1}{\sqrt{2}}\pi^0 + \frac{1}{\sqrt{6}}\eta & \pi^+ & K^+ \\ \pi^- & -\frac{1}{\sqrt{2}}\pi^0 + \frac{1}{\sqrt{6}}\eta & K^0 \\ K^- & \bar{K}^0 & -\sqrt{\frac{2}{3}}\eta \end{pmatrix}, \quad (11)$$

$$B = \begin{pmatrix} \frac{1}{\sqrt{2}}\Sigma^0 + \frac{1}{\sqrt{6}}\Lambda & \Sigma^+ & p \\ \Sigma^- & -\frac{1}{\sqrt{2}}\Sigma^0 + \frac{1}{\sqrt{6}}\Lambda & n \\ \Xi^- & \Xi^0 & -\sqrt{\frac{2}{3}}\Lambda \end{pmatrix}, \quad (12)$$

and m_q is the quark mass matrix

$$m_q = \begin{pmatrix} 0 & 0 & 0 \\ 0 & 0 & 0 \\ 0 & 0 & m_s \end{pmatrix}, \quad (13)$$

where we assume massless up and down quarks ($m_u = m_d = 0$) and m_s is the finite current mass of strange quark. By expanding U in terms of meson fields, we can obtain the kinetic energy and mass of meson fields which correspond to the first and second term, respectively in the first line of Eq. (8). Note that there are other interaction terms with higher order in the meson fields due to the SU(3) symmetry. The constant c in the mass term can be determined from the relation $m_K^2 = 2c m_s/f_\pi^2$. The third term in the first line of Eq. (8) represents the kinetic energy of octet baryons. The second and third lines in Eq. (8) represent the interactions among mesons and baryons. We use $F = 0.44$ and $D = 0.81$ which are fixed by weak nucleon and semileptonic hyperon decays. For $a_1 m_s$ and $a_2 m_s$, we quote the values given in Ref. [13], where

$$a_1 m_s = -67 \text{ MeV}, \quad (14)$$

$$a_2 m_s = 134 \text{ MeV}. \quad (15)$$

In principle, the value of a_3 can be fixed by using the strangeness content of the proton $\langle \bar{s}s \rangle_p$ or the kaon-nucleon sigma term Σ^{KN} ;

$$m_s \langle \bar{s}s \rangle_p = -2(a_2 + a_3)m_s, \quad (16)$$

$$\Sigma^{KN} = -\frac{1}{2}(a_1 + 2a_2 + 4a_3)m_s. \quad (17)$$

However, due to the uncertainties in these quantities, we choose four different values of $a_3 m_s$, -134 , -178 , -222 and -310 MeV, which correspond to the strangeness content $\langle \bar{s}s \rangle_q = 0$, 0.05 , 0.1 and 0.2 , respectively.

The amount of kaon condensation can be determined from local flavor changing β -equilibrium, e.g., $n \leftrightarrow p + K^-$. This chemical equilibrium implies $\mu_n = \mu_p + \mu_{K^-}$, where μ_i denotes the chemical potential of particle ‘ i ’. For the simplicity, we use $\mu_K = \mu_{K^-}$ afterward. Other equilibrium conditions will be discussed in the next subsection. With the s-wave interactions only, the kaon condensate can be characterized by the expectation value [14]

$$\langle K^- \rangle = v_K e^{-i\mu_K t}, \quad (18)$$

where the amplitude v_K determines the magnitude of the condensate. Since the kaon field appears non-linear in Eq. (9), it is convenient to introduce a new parameter θ by

$$\theta \equiv \sqrt{2} \frac{v_K}{f_\pi}. \quad (19)$$

Expanding Eq. (8) in terms of meson and baryon fields and retaining the terms relevant to kaons and nucleons, we obtain the Lagrangian for the kaon and kaon-nucleon interactions as

$$\begin{aligned} \mathcal{L}_K = & f_\pi^2 \frac{\mu_K^2}{2} \sin^2 \theta - 2m_K^2 f_\pi^2 \sin^2 \frac{\theta}{2} \\ & - n^\dagger n [-\mu_K + (2a_2 + 4a_3)m_s] \sin^2 \frac{\theta}{2} \\ & - p^\dagger p [-2\mu_K + (2a_1 + 2a_2 + 4a_3)m_s] \sin^2 \frac{\theta}{2}. \end{aligned} \quad (20)$$

Taking μ_K as a Lagrangian multiplier to account for the charge neutrality condition of the neutron star matter, Hamiltonian density is derived from the kaon Lagrangian which is given by Eq. (20). We obtain the Hamiltonian density for the kaon as

$$\begin{aligned} \mathcal{H}_K = & -f_\pi^2 \frac{\mu_K^2}{2} \sin^2 \theta + 2m_K^2 f_\pi^2 \sin^2 \frac{\theta}{2} + \mu_K \rho_p \\ & - \mu_K (\rho + \rho_p) \sin^2 \frac{\theta}{2} + a_{K1} \rho_p \sin^2 \frac{\theta}{2} + a_{K2} \rho \sin^2 \frac{\theta}{2}, \end{aligned} \quad (21)$$

where $a_{K1} = 2a_1 m_s$ and $a_{K2} = (2a_2 + 4a_3)m_s$.

In addition to the hadron parts discussed so far, leptonic terms should be added for the complete description of EoS. We consider both electrons and muons in this work, and their Hamiltonian densities are given as

$$\tilde{\mathcal{H}}_e = \frac{\mu_e^4}{4\pi^2} - \mu_e \rho_e, \quad (22)$$

$$\tilde{\mathcal{H}}_\mu = H(|\mu_\mu| - m_\mu) \left\{ \frac{m_\mu^4}{8\pi^2} \left[(2x_\mu^2 + 1)x_\mu \sqrt{x_\mu^2 + 1} - \ln \left(x_\mu + \sqrt{x_\mu^2 + 1} \right) \right] - \mu_\mu \rho_\mu \right\}, \quad (23)$$

where $\rho_e = \mu_e^3/3\pi^2$, H is the Heaviside step function, $\rho_\mu = k_\mu^3/3\pi^2$, $\mu_\mu = \sqrt{k_\mu^2 + m_\mu^2}$, and $x_\mu = k_\mu/m_\mu$ with the Fermi momentum of muon k_μ . Note that we allow negative values of $\mu_{e,\mu}$ in order to take into account the contributions of e^+ and μ^+ .

C. Equilibrium conditions

As mentioned earlier, ten parameters in the nucleon Hamiltonian Eq. (3) are determined by fitting to the properties of finite nuclei for a given density ρ . After determining the ten parameters, we have only one independent variable ρ_p with the constraint $\rho = \rho_n + \rho_p$. In the following, we use $x \equiv \rho_p/\rho$ for the simplicity. In this work, we assume that only proton and neutron contribute to the baryon density even at the high-density core of neutron star. In the Hamiltonians for kaons and leptons, Eqs. (21) to (23), there are four independent variables μ_K , v_K (or θ), μ_e , and μ_μ . By neglecting contributions from (anti)neutrinos which leave the system, we can set $\mu_K = \mu_\mu = \mu_e$. As a result, we have only three independent variables x , μ_e , and θ which are determined by minimizing the total energy density given as

$$\epsilon = \epsilon_N + \epsilon_K + \epsilon_e + \epsilon_\mu. \quad (24)$$

Three coupled equations are solved for x , μ_e , and θ ,

$$\frac{\partial \epsilon}{\partial x} = 0 : \mu_e = (\mu_n^{\text{SHF}} - \mu_p^{\text{SHF}}) \sec^2 \frac{\theta}{2} - a_{K1} \tan^2 \frac{\theta}{2}, \quad (25)$$

$$\frac{\partial \epsilon}{\partial \mu_e} = 0 : f_\pi^2 \mu_e^2 \sin^2 \theta + (\rho + \rho_p) \sin^2 \frac{\theta}{2} = \rho_p - \rho_e - \rho_\mu, \quad (26)$$

$$\frac{\partial \epsilon}{\partial \theta} = 0 : -\mu_e^2 \cos \theta + m_K^2 - \frac{1}{2f_\pi^2} \mu_e (\rho + \rho_p) + \frac{a_{K1}}{2f_\pi^2} \rho_p + \frac{a_{K2}}{2f_\pi^2} \rho = 0, \quad (27)$$

where $\mu_{n,p}^{\text{SHF}}$ are the chemical potential of nucleon in the general SHF model only. Eqs. (25) and (26) are the beta equilibrium and local charge neutrality condition, respectively with kaons included. Note that Eq. (27) is valid only for the densities beyond the critical density

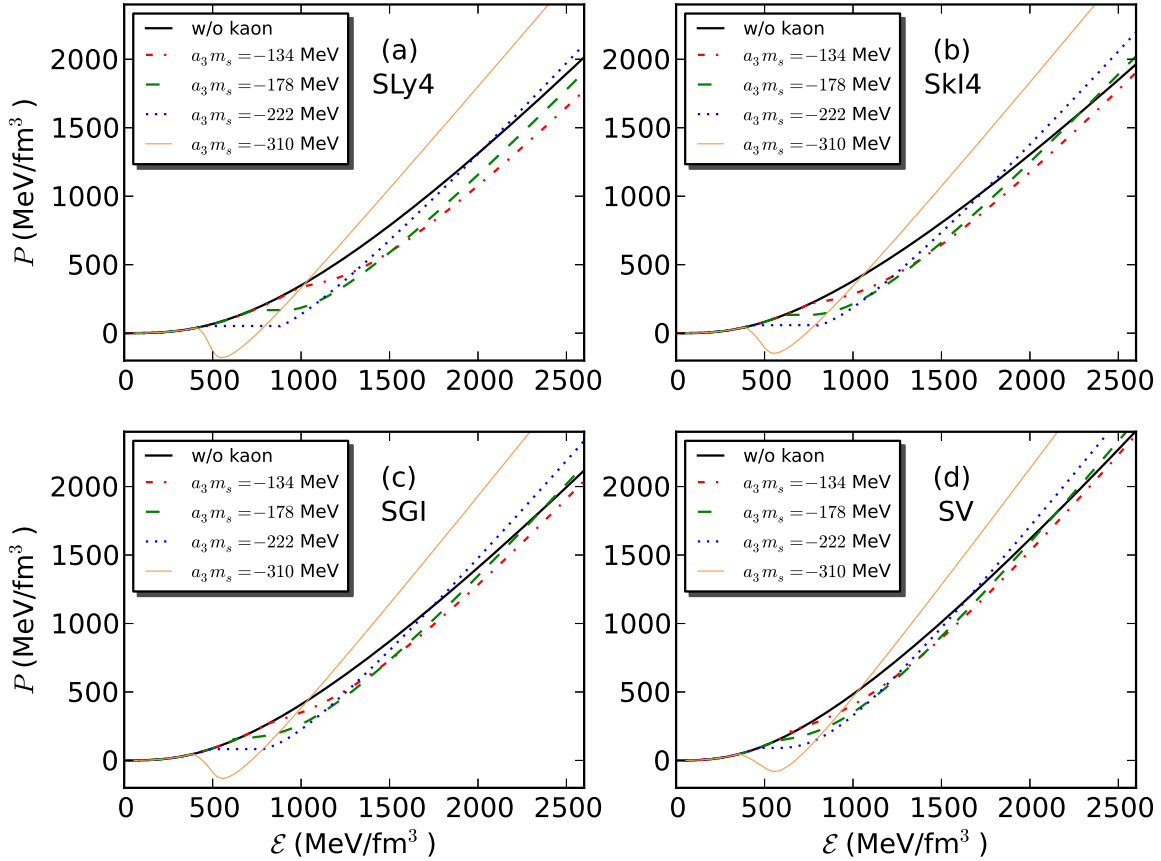


FIG. 1: Equation of state for each of four SHF models (color figures are available in online version). For $a_3 m_s = -178$ and -222 MeV, Maxwell construction is used to make the pressure constant for the unstable energy density region. In case of $a_3 m_s = -310$ MeV, Maxwell construction is not possible since the kaon condensation makes the system too soft and thermodynamically unstable for the low energy density region, hence the neutron star has finite surface density.

where $\theta \neq 0$. Once these equations are solved, we can calculate the pressure from the thermodynamic relation

$$p = \rho^2 \frac{\partial}{\partial \rho} \left(\frac{\epsilon}{\rho} \right), \quad (28)$$

and determine the EoS as a function of density ρ .

Model	$a_3m_s = -134$ MeV	$a_3m_s = -178$ MeV	$a_3m_s = -222$ MeV	$a_3m_s = -310$ MeV
SLy4	0.8580 (5.36)	0.6887 (4.30)	0.5689 (3.56)	0.4183 (2.61)
SkI4	0.6813 (4.26)	0.5830 (3.64)	0.5070 (3.17)	0.3962 (2.48)
SGI	0.7002 (4.52)	0.5890 (3.80)	0.5060 (3.26)	0.3921 (2.53)
SV	0.5944 (3.83)	0.5139 (3.32)	0.4512 (2.91)	0.3608 (2.33)

TABLE II: Critical densities in unit of fm^{-3} (values in parentheses are in unit of ρ_0) for four SHF models with kaon condensation included. The critical density for kaon condensation decreases as a_3m_s decreases, i.e., the strangeness content increases.

III. NEUTRON STARS WITH KAON CONDENSATION

A. Equation of state and critical densities

Equation of state of nuclear matter, which in general is the relation between pressure and energy density, can be calculated from Eqs. (24) and (28). We employ four Skyrme force models (SLy4, SkI4, SGI, and SV) to calculate the uniform nuclear matter EoS ($\rho > 0.08 \text{ fm}^{-3}$). In the regime where the density is smaller than the density of uniform nuclear matter ($\rho < 0.08 \text{ fm}^{-3}$), we use liquid droplet model to treat heavy nuclei and free gas of neutrons and electrons (see Appendix). Once we choose one specific SHF model for the EoS calculation of the entire neutron star, we apply the same model to both the uniform nuclear matter (high density regime) and the non-uniform lattice nuclear matter (low density regime).

Fig. 1 shows the EoS for each of four models with four values of a_3m_s that we select. Note that the local charge neutrality is assumed for both cases with and without kaon condensation. The results obtained without kaon condensation (black thick solid line in each panel) show that SLy4 is the softest while SV is the stiffest EoS, which can be expected from the values of L and K in Table I. As the energy density increases from 0, kaon starts to condense at the density where the curves with kaon deviate from those without kaon. Table II summarizes the numerical results for the critical densities at which the kaon condensation appears. Numbers in the parentheses denote the critical densities in unit of ρ_0 for each model. As indicated in the Fig. 1 and Table II, kaons condense earlier with smaller a_3m_s

values (i.e., larger strangeness content) for all models. Table II shows that the change of the critical densities resulting from change of a_3m_s is the largest for SLy4 which has the softest EoS among the four models. This implies that the softer nuclear models are more sensitive to the existence of kaons. This sensitivity can also be deduced from the EoS in Fig. 1 by noting that the width of band between the curves for $a_3m_s = -134$ MeV and -222 MeV becomes narrower with a stiffer nuclear EoS. In Fig. 1, with $a_3m_s = -134$ MeV, kaons soften the EoS in the entire energy density region. However, for other values of a_3m_s , kaons harden the EoS at very high energy densities. Nonlinear chiral model for the meson-baryon interactions has been already employed in the work by Thorsson et al. [15]. By assuming simple functional forms for the description of nuclear forces and considering various compression modulus in the range of $K = 120 - 240$ MeV, they obtained critical densities in the range of $\rho_{\text{crit}} = (2.30 - 4.95)\rho_0$, which are similar to what we obtain with more realistic nuclear models in this work.

After the formation of kaon condensation, we have an unstable part in the EoS where the derivative of pressure with respect to the energy density is negative. This unstable region can be treated by either Maxwell construction or Gibbs condition. In this work we adopt the Maxwell constructions, and the flat parts in the EoS are the consequences of the Maxwell constructions. However, the Maxwell construction is not possible for $a_3m_s = -310$ MeV because the pressure decreases so much that the mean value of the pressure is negative for the low density region. Hence the neutron star has finite surface density and the resulting mass and radius of neutron star with $a_3m_s = -310$ MeV are far from the current observations [6, 7]. Therefore, we do not include the results with $a_3m_s = -310$ MeV in the later discussion.

B. Particle fractions

In Fig. 2, we show the particle fractions defined as the densities of each particle divided by the baryon density, for the SkI4 model. Both kaon and proton densities increase very rapidly right after the critical densities due to the local charge neutrality. Note that the local charge neutrality is implied in this figure and, even though we plot particle fractions for all densities, there exist density gaps in the interior of neutron stars due to the Maxwell construction. In this figure, as a_3m_s decreases, both proton and kaon fractions increase

beyond neutron fraction, which enhances the contribution of the symmetry energy to the EoS. Unlike leptons, kaon is not constrained by the Pauli blocking, and most of the leptons are suppressed by kaons at high densities making the fraction of kaons almost equal to that of protons.

C. Mass and radius of neutron star

The relation between mass and radius of cold neutron star can be obtained by solving the Tolman-Oppenheimer-Volkoff (TOV) equations numerically,

$$\frac{dp}{dR} = -\frac{G(M(R) + 4\pi R^3 p/c^2)(\epsilon + p)}{R(R - 2GM(R)/c^2)c^2}, \quad (29)$$

$$\frac{dM}{dR} = 4\pi \frac{\epsilon}{c^2} R^2, \quad (30)$$

where ϵ and p denote the energy density and pressure, respectively.

In Fig. 3 we show the mass of neutron stars as a function of radius for four SHF models. Thick blue and thick orange solid straight lines indicate the mass range of PSR J1614–2230 and J0348+0432, respectively [6, 7] and filled circles with error bars denote the allowed mass and radius ranges obtained from the analysis by Steiner et al. [16]. Again, Fig. 3 confirms that the maximum mass increases as the stiffness of EoS increases.

Table III summarizes the maximum mass of neutron stars predicted from four SHF models with kaon condensation included. For the comparison, the maximum mass obtained from the same models without kaon condensation (from Tab. I) is also shown in the last column of Tab. III. For $a_3 m_s = -134$ MeV, the effect of kaon condensation on the maximum mass of neutron stars is rather weak, reducing the maximum mass by less than 4 %. With smaller $a_3 m_s$ values, the curves deviate more dramatically from those without kaons. Note that in all models except SV, the existence of the unstable part with $a_3 m_s = -222$ MeV, which is near the kink at $R = 11 - 12$ km having a positive slope in the mass-radius curve (Fig. 3), is an artifact of the Maxwell construction. With the Gibbs condition, the kink generally disappears and the curve becomes smooth (see e.g. [17]). Since the Gibbs condition only affects the unstable region, our conclusion in this work remains unchanged.

In Fig. 3, the results with $a_3 m_s = -222$ MeV are not consistent with either of the observed neutron star masses or the mass-radius ranges obtained by Steiner et al.[16], regardless of

TABLE III: Maximum mass of neutron star (in unit of M_\odot) in the presence of kaon for each model.

Model	$a_3 m_s = -134$ MeV	$a_3 m_s = -178$ MeV	$a_3 m_s = -222$ MeV	no kaon
SLy4	1.99	1.83	1.79	2.07
SkI4	2.07	1.91	1.85	2.19
SGI	2.20	2.04	1.94	2.25
SV	2.39	2.24	2.12	2.44

any choice of the SHF models. In contrast, with $a_3 m_s = -134$ MeV, both SLy4 and SkI4 are consistent with observations.

Recently, Guillot *et al.* [18] have measured small radii of neutron stars ($R_\infty = 9.1_{-1.5}^{+1.3}$ km with the 90% confidence level: see Ref. [19], however, for an alternative interpretation of this data) using the thermal spectra from quiescent low-mass X-ray binaries inside five globular clusters. The smaller radii of neutron stars that they measured prefer the softer EoS such as Wiringa *et al.*'s [19] and rule out most of the presently popular EoS. It is interesting that our results with kaon condensation could explain the existence of such a neutron star that has a radius of ~ 9 km and a mass of $\sim 2.0 M_\odot$ (e.g., see the $a_3 m_s = -222$ MeV case of SGI in the panel (c) of Fig. 3).

IV. CONCLUSION

This work is motivated by the fact that many SHF models, which are excellent in reproducing the properties of known nuclei, are inconsistent in predicting nuclear matter properties at supra-nuclear densities. We select four SHF models that are consistent with recent observations of neutron star masses [6, 7] in order to investigate and understand the effect of kaon condensation. Since the interactions of kaon in nuclear medium are quite uncertain, we employ four different parameter sets to cover a wide range of kaon interactions.

As one can see in Fig. 3, SLy4 and SkI4 are consistent with the recent constraints [6, 7, 16] even without kaon condensation. Adding kaons to these models, the mass-radius relation with kaon deviates from the those without kaons more drastically for smaller $a_3 m_s$ values. As a result, the behavior with $a_3 m_s = -222$ MeV satisfies the mass-radius relation

constraints in a limited manner. This result shows that the observation of the neutron star can provide constraints on the strangeness content of the proton, and our result implies that kaon condensation, if it occurs, should occur only for heavy neutron stars ($> 1.9M_\odot$), with a_3m_s being greater than -178 MeV (or the strangeness content being smaller than 0.05). This small allowed value of strangeness content of the proton is in accordance with experiments [20], lattice calculation [21], and a recent updated calculation with a chiral effective theory [22]. This would be also consistent with the recent observation of Cas A and its cooling simulation [23] because kaon condensation does not affect thermal evolution of neutron stars with smaller mass ($M < 1.9M_\odot$).

We have discussed the contribution of strangeness by focusing only on the kaon in this work, but we have to consider hyperons as well for the consistency. In the current SHF approach, to our knowledge, there are more than 10 models for hyperon-nucleon interactions and 3 models for the hyperon-hyperon interactions in nuclear matter. Our recent analysis shows that the EoS at high densities and the resulting mass and radius of neutron star are also highly sensitive to the hyperon-nucleon and hyperon-hyperon interactions in nuclear medium. We will present the work with hyperons in the future.

Acknowledgments

We would like to thank the referee for the valuable criticisms and comments. CHH is grateful to E. Hiyama for useful comments about the recent results in the hypernuclear interactions. Work of CHH and YL was supported by the Basic Science Research Program through the National Research Foundation of Korea (NRF) funded by the Ministry of Education, Science and Technology Grant No. 2010-0023661. YL was also supported by the Rare Isotope Science Project funded by the Ministry of Science, ICT and Future Planning (MSIP) and National Research Foundation (NRF) of Korea. CHL was supported by the BAERI Nuclear R & D program (M20808740002) of MEST/KOSEF and the Financial Supporting Project of Long-term Overseas Dispatch of PNU's Tenure-track Faculty, 2013. KK was supported by the year 2013 Research Fund of the Ulsan National Institute of Science and Technology (UNIST).

Appendix A: Heavy nuclei with dripped neutrons

We follow the discussion of Lattimer & Swesty [24]. The total energy density (without electron contribution) is given by

$$F = un_i f_i + \frac{3s(u)}{r_N} [\sigma(x) + \mu_s \nu_n] + \frac{4\pi}{5} (r_N n_i x_i e)^2 c(u) + (1-u)n_{no} f_o, \quad (\text{A1})$$

where u is a volume fraction of heavy nuclei to Wigner-Seitz cell, n_i is the density of heavy nuclei inside, f_i is the energy per baryon of the heavy nuclei, $s(u)$ is surface shape factor, r_N is the radius of heavy nuclei, $\sigma(x)$ is a surface tension as a function of proton fraction x , μ_s is the neutron chemical potential on the surface, ν_n is the areal neutron density on the surface, x_i is the proton fraction of heavy nuclei, $c(u)$ is the Coulomb shape function, n_{no} is the neutron density outside of heavy nuclei, and f_o is the energy per baryon outside of the heavy nuclei.

We employ Lagrange-Multiplier method with constraints (baryon number density and charge neutrality), thus for given baryon number density (n) and proton fraction (Y_p), we have

$$G = F + \lambda_1 \left[n - un_i - 3s(u) \frac{\nu_n}{r_N} - (1-u)n_{no} \right] + \lambda_2 (nY_p - un_i x_i). \quad (\text{A2})$$

In the above equations, unknowns are n_i , x_i , r_N , x , $\frac{\nu_n}{r_N}$, u , and n_{no} .

$$\frac{\partial G}{\partial n_i} = 0 : \quad u(\mu_{n_i} - x_i \hat{\mu}_i) + \frac{8\pi}{5} (r_N x_i e)^2 n_i c(u) - \lambda_1 u - \lambda_2 u x_i = 0, \quad (\text{A3})$$

$$\frac{\partial G}{\partial x_i} = 0 : \quad -un_i \hat{\mu}_i + \frac{8\pi}{5} (r_N n_i e)^2 x_i c(u) - \lambda_2 un_i = 0, \quad (\text{A4})$$

$$\frac{\partial G}{\partial r_N} = 0 : \quad -\frac{3s(u)}{r_N^2} \sigma + \frac{8\pi}{5} (n_i x_i e)^2 c(u) = 0, \quad (\text{A5})$$

$$\frac{\partial G}{\partial x} = 0 : \quad \frac{3s(u)}{r_N} \left(\frac{\partial \sigma}{\partial x} + \nu_n \frac{\partial \mu_s}{\partial x} \right) = 0, \quad (\text{A6})$$

$$\frac{\partial G}{\partial (\nu_n/r_N)} = 0 : \quad 3s(u)(\mu_s - \lambda_1) = 0, \quad (\text{A7})$$

$$\frac{\partial G}{\partial u} = 0 : \quad n_i f_i + \frac{3s'}{r_N} (\sigma + \mu_s \nu_n) + \frac{4\pi}{5} (r_N n_i x_i e)^2 c' - \lambda_1 (n_i + 3s' \frac{\nu_n}{r_N} - n_{no}) - \lambda_2 n_i x_i = 0, \quad (\text{A8})$$

$$\frac{\partial G}{\partial n_{no}} = 0 : \quad (1-u)\mu_{no} - (1-u)\lambda_1 = 0, \quad (\text{A9})$$

$$\frac{\partial G}{\partial \lambda_1} = 0 : \quad n_i - un_i - 3s(u) \frac{\nu_n}{r_N} = 0, \quad (\text{A10})$$

$$\frac{\partial G}{\partial \lambda_2} = 0 : \quad nY_p - un_i x_i = 0, \quad (\text{A11})$$

where $\hat{\mu}_i = \mu_{ni} - \mu_{pi}$. μ_{ni} and μ_{pi} are neutron and proton chemical potential inside of the heavy nuclei, respectively.

Eq. (A3) $\times n_i$ - (A4) $\times x_i$ gives $\lambda_1 = \mu_{ni}$. From Eq. (A7), we have $\lambda_1 = \mu_s$. From Eq. (A9), $\lambda_1 = \mu_{no}$, so $\mu_{ni} = \mu_{no} = \mu_s$.

Similarly we have λ_2 from Eq. (A4),

$$\begin{aligned}\lambda_2 &= -\hat{\mu}_i + \frac{1}{un_i} \frac{8\pi}{5} (r_N n_i e)^2 x_i c(u) \\ &= -\hat{\mu}_i + \frac{1}{un_i x_i} \frac{2}{3} \beta \mathcal{D}(u),\end{aligned}\tag{A12}$$

where $\beta = 9\left(\frac{\pi e^2 x_i^2 n_i^2 \sigma^2}{15}\right)^{1/3}$, and $\mathcal{D} = [c(u)s^2(u)]^{1/3}$ is a geometric shape function which corresponds to nuclear pasta phase in liquid droplet model [24].

Finally, if we plug Eq. (A12) into Eq. (A8) then we get,

$$\begin{aligned}n_i f_i + \beta \mathcal{D}' - \mu_{ni} n_i + n_i x_i \hat{\mu}_i - \frac{2}{3u} \beta \mathcal{D} + \mu_{no} n_{no} - n_{no} f_o &= 0 \\ \Rightarrow P_i - P_o - \beta \left(\mathcal{D}' - \frac{2\mathcal{D}}{3u} \right) &= 0,\end{aligned}\tag{A13}$$

where P_i (P_o) is pressure inside (outside) of the heavy nuclei. Thus, we have four equations to solve

$$\begin{aligned}P_i - P_o - \beta \left(\mathcal{D}' - \frac{2\mathcal{D}}{3u} \right) &= 0, \\ un_i x_i - n Y_p &= 0, \\ un_i + \frac{2\beta}{3\sigma} \mathcal{D} \nu_n + (1-u)n_{no} - n &= 0, \\ \mu_{ni} - \mu_{no} &= 0,\end{aligned}\tag{A14}$$

with four unknowns, u (or $\ln u$), n_i , n_{no} (or $\ln n_{no}$), and x_i .

Thermodynamic quantities for this case is given by the same formalism with hot dense matter but without alpha particle and translational term, so

$$\begin{aligned}\hat{\mu} &= \hat{\mu}_i - \frac{2}{3un_i x_i} \beta \mathcal{D}, \\ \mu_n &= \mu_{no}, \\ P &= P_o - \beta (\mathcal{D} - u \mathcal{D}').\end{aligned}\tag{A15}$$

In case of neutron star outer crust, we can construct eq. (A1) without n_{no} and follow the

same methodology with the case of neutron star inner crust.

-
- [1] B. A. Brown, Phys. Rev. Lett. **85**, 5296 (2000).
 - [2] ‘PhD thesis’, Yeunhwan Lim (2012).
 - [3] L. Mornas, Eur. Phys. J. A **24**, 293 (2005).
 - [4] N. Guleria, S. K. Dhiman, and R. Shyam, Nucl. Phys. A **886**, 71 (2012).
 - [5] C.-Y. Ryu, C. H. Hyun, C.-H. Lee, Phys. Rev. C **84**, 035809 (2011).
 - [6] P. Demorest, T. Pennucci, S. Ransom, M. Roberts, and J. W. T. Hessels, Nature **467**, 1081 (2010).
 - [7] J. Antoniadis *et al.*, Science **340**, 448 (2013).
 - [8] C. Y. Ryu, C. H. Hyun, S. W. Hong, and B. T. Kim, Phys. Rev. C **75**, 055804 (2007).
 - [9] A. W. Steiner, M. Prakash, J. M. Lattimer, and P. J. Ellis, Phys. Rep. **411**, 325 (2005).
 - [10] M. Kortelainen, T. Lesinski, J. More , W. Nazarewicz, J. Sarich, N. Schunck, M. V. Stoitsov, and S. Wild, Phys. Rev. C **82**, 024313 (2010).
 - [11] R. Knorren, and M. Prakash, and P. J. Ellis Phys. Rev. C **52**, 3470 (1995).
 - [12] D. B. Kaplan, and A. E. Nelson, Phys. Lett. B **175**, 57 (1986).
 - [13] B. Thorsson, M. Prakash, and J. M. Lattimer, Nucl. Phys. A **572**, 693 (1994).
 - [14] G. Baym, Phys. Rev. Lett. **30**, 1340 (1973).
 - [15] V. Thorsson, M. Prakash, and J. M. Lattimer, Nucl. Phys. A **572**, 693 (1994).
 - [16] A. W. Steiner, J. M. Lattimer, and E. F. Brown, ApJ **722**, 33 (2010).
 - [17] C. Y. Ryu, C. H. Hyun, and S. W. Hong, J. Korean Phys. Soc. **54**, 1448 (2009).
 - [18] S. Guillot, M. Servillat, N. A. Webb, and R. E. Rutledge, ApJ **772**, 7 (2013).
 - [19] R. B. Wiringa, V. Fiks, and A. Fabrocini, Phys. Rev. C **38**, 1010 (1988).
 - [20] D. S. Armstrong, and R. D. McKweon, Ann. Rev. Nucl. Part. Sci, **62**, 337 (2012).
 - [21] T. Doi, M. Deka, S.-J. Dong, T. Draper, K.-F. Liu, D. Mankame, N. Mathur, and T. Streuer, Phys. Rev. D **80**, 094503 (2009).
 - [22] P. Wang, D. B. Leinweber, and A. W. Thomas, arXiv:1312.3375 [hep-ph].
 - [23] D. Page, M. Prakash, J. M. Lattimer, and A. W. Steiner, Phys. Rev. Lett.**106**, 081101 (2011).
 - [24] J. M. Lattimer and F. D. Swesty, Nucl. Phys. A **535**, 331 (1991).

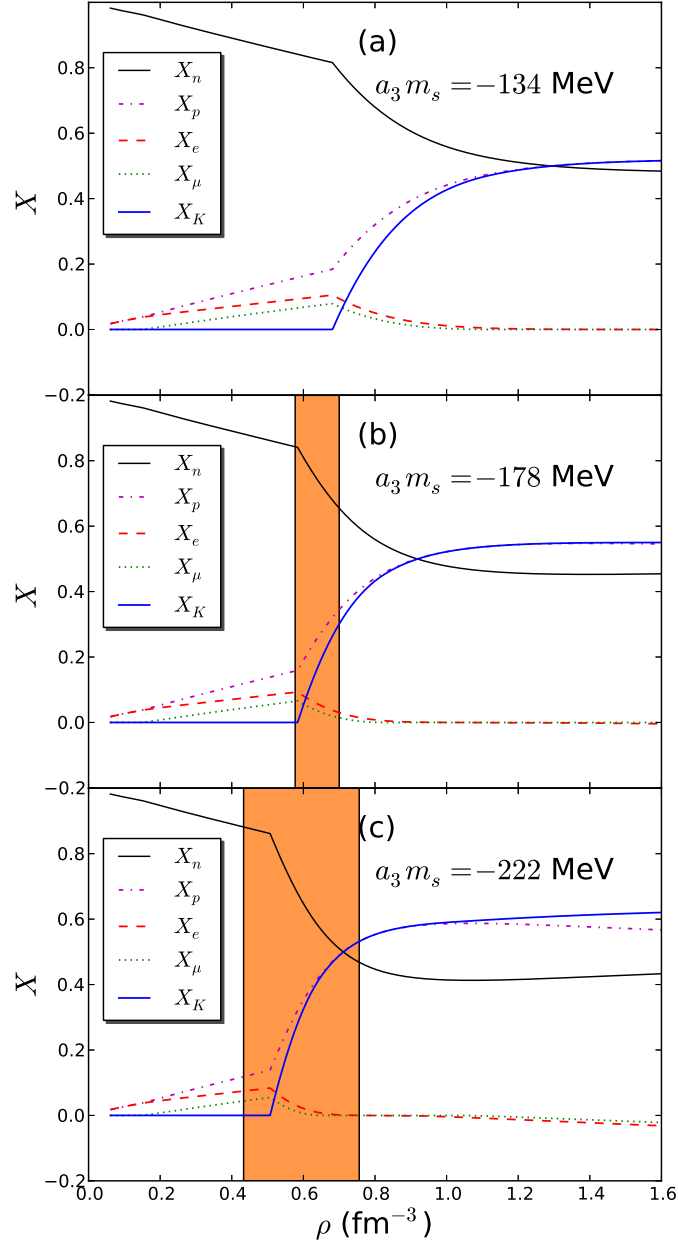


FIG. 2: Particle fractions of nuclear matter defined as the densities of each particle divided by baryon density for the SkI4 model with kaon condensation included (color figures are available in online version). Negative fraction means anti-particle corresponding to each particle. Band intervals in (b) and (c) represent the Maxwell construction area where the pressure is constant.

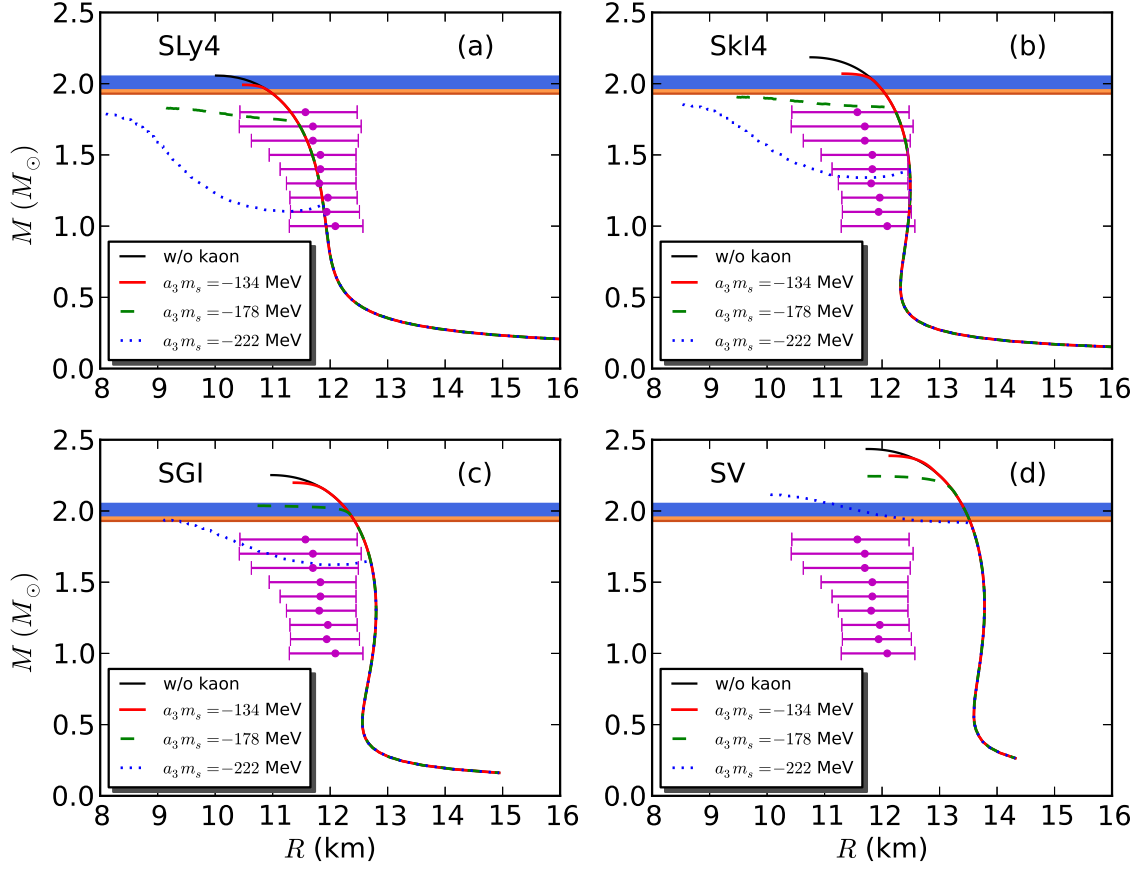


FIG. 3: Mass-radius curve for each of four SHF models (color figures are available in online version). Thick blue and thick orange solid straight lines are recent observations [6, 7]. Filled circles with error bars denote the allowed mass and radius ranges obtained from the analysis by Steiner et al. [16].